Active Site Dynamics in the Lead-Dependent Ribozyme†

Charles G. Hoogstraten,‡ Jeffrey R. Wank, and Arthur Pardi*

Department of Chemistry and Biochemistry, University of Colorado at Boulder, Campus Box 215, Boulder, Colorado 80309

Received April 4, 2000; Revised Manuscript Received June 14, 2000

ABSTRACT: Conformational dynamics are an important property of ribozymes and other RNA molecules but there is currently only limited information on the relationship between dynamics and RNA function. A recent structural study of the lead-dependent ribozyme, known as the leadzyme, showed significant dynamics at the active site and indicated that a structural rearrangement is required for the reaction to proceed from the ground to the transition state. In this work, microsecond-to-millisecond dynamics of the leadzyme are probed by analysis of the power dependence of ^{13}C NMR relaxation times in the rotating frame ($T_{1\rho}$). These results revealed a wide range of conformational dynamics for various residues in the leadzyme. For residue A25 in the active site, the power dependence of $T_{1\rho}$ yielded an exchange lifetime similar to that previously measured by line-shape analysis, and provides an important calibration of this $T_{1\rho}$ methodology for probing the dynamics of macromolecules. Strong evidence was also found for a previously suggested dynamic network of hydrogen bonds stabilizing the GAAA tetraloop motif. Within the active site of the leadzyme, internal motions are observed on a wide variety of time scales, suggesting a complex landscape of accessible states, and potential correlations between observed motions and catalytic function are discussed. These results demonstrate that the power dependence of ^{13}C $T_{1\rho}$ relaxation times provides a valuable method for probing dynamics in nucleic acids.

The recent dramatic progress in RNA structural biology (*1*−*3*) has emphasized the key role that conformational dynamics play in the function of many RNA molecules. In particular, reactive groups in the hammerhead ribozyme (*4*−*6*) and the lead-dependent ribozyme (*7*, *8*) are not positioned for in-line nucleophilic attack, as proposed for the phosphoryl transfer mechanism (*9*). Therefore, these ribozymes rely on thermal fluctuations to proceed from the highly populated equilibrium conformation to a low-population active conformation that is required for catalysis. Conformational transitions also play key roles in RNA recognition of proteins and other ligands (*10*), in the function of the ribosome (*11*) and the spliceosome (*12*, *13*). Thus, a full understanding of the structure−function correlations of catalytic RNAs and ribonucleoproteins requires characterization of both the static structure and conformational dynamics of the molecule.

A recent NMR structural study of the lead-dependent ribozyme, or leadzyme (*7*), found that the most populated conformation in solution is not positioned for approach to the presumed transition state, and that a conformational rearrangement is therefore necessary for catalysis. The active-site internal loop of the leadzyme contains an intriguing mixture of stable structural features and conformational dynamics, as assayed by both chemical probing and NMR techniques (see Figure 1). Additional information on the ensemble of structures present in solution will be important for elucidating the catalytic mechanism of this ribozyme. In this work, the power dependence of ^{13}C $T_{1\rho}$ spin relaxation times for the purine C8 and adenine C2 resonances are used to probe the conformational dynamics of the leadzyme on microsecond-to-millisecond time scales. The dynamics for one site had been previously characterized by line-shape analysis (*14*, *15*), and comparison of the lifetime obtained here by the ^{13}C $T_{1\rho}$ measurements provides a valuable cross-validation of the more generally applicable ^{13}C $T_{1\rho}$ spin relaxation technique. Conformational dynamics on a variety of time scales are observed for residues in the active site of the leadzyme.

Solution NMR is well adapted to studying macromolecular dynamics on a variety of time scales (*16*). Specifically, heteronuclear spin relaxation measurements are sensitive to dynamics ranging from picoseconds to milliseconds (*17*−*19*). Conformational dynamics associated with molecular function in ribozymes will likely occur on a time scale of microseconds to milliseconds and involve thermally induced "exchange" between two or more relatively well-defined conformational states. The standard model-free analysis of relaxation data (*20*, *21*) is not well suited to the study of such dynamics, since exchange on this time scale is only represented by R_{ex}, which represents an error term used to account for inconsistently short values for the transverse relaxation time. Thus it is often difficult to unambiguously interpret R_{ex}. For example, apparent R_{ex} contributions have been found to arise instead from anisotropy of molecular diffusion (*22*).

Macromolecular dynamics in the microsecond-to-millisecond regime can be more rigorously studied by analysis

† This work was supported by NIH Grant AI33098 to A.P. and a Helen Hay Whitney Foundation Postdoctoral Fellowship to C.G.H. We also thank the Colorado RNA Center for support of RNA research on the Boulder campus.

* To whom correspondence should be addressed. E-mail: arthur.pardi@colorado.edu.

‡ Current address: Department of Chemistry, University of California at Davis, One Shields Avenue, Davis, CA, 95616.

10.1021/bi0007627 CCC: $19.00
Published on Web 07/22/2000

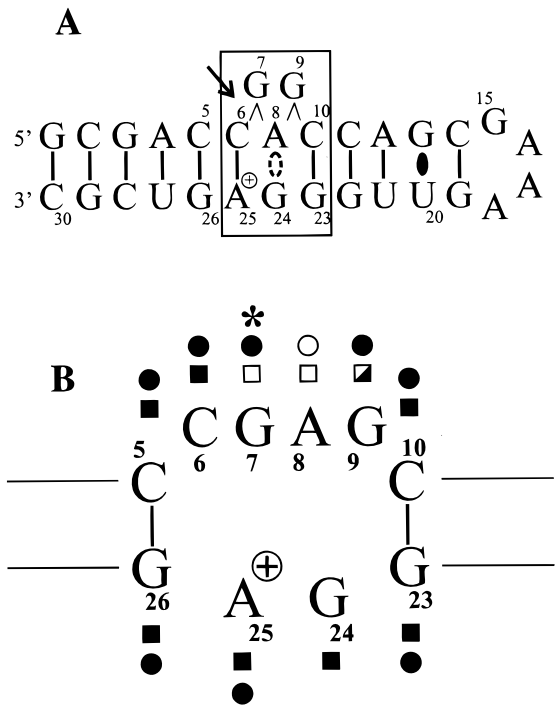

FIGURE 1: (A) Sequence and schematic structure of the lead-dependent ribozyme construct used here (*55*). The active-site internal loop is boxed, the scissile phosphate is indicated by an arrow, and the adenine residue protonated at the experimental pH is marked. Dotted lines connecting A8 and G24 indicate that, in the ribozyme ground state, these residues were found to be within the helix and mutually interacting but did not exhibit a unique base pair (*7*). (B) Expanded view of the active site showing data relating to dynamic features. The symbols correspond to the following properties: filled box, protection from chemical modification upon ribozyme folding; open box, no protection; half-filled box, partial protection; filled circle, single sugar pucker conformation (C3′-endo or C2′-endo); open circle, averaged sugar pucker; asterisk, NOEs to base proton inconsistent with a single conformation (*7*, *39*, *56*).

of the power dependence of $T_{1\rho}$. For a system exchanging between two states, the transverse relaxation rate under spin-locked conditions, $R_{1\rho}$ is described by eq 1 (*23*, *24*):

$$R_{1\rho} = \frac{1}{T_{1\rho}} = \frac{1}{T_{1\rho}^{\infty}} + p_a p_b (\Delta\omega)^2 \frac{\tau_{ex}}{1 + \omega_1^2 \tau_{ex}^2} \qquad (1)$$

where $T_{1\rho}$ is the measured relaxation time, $T_{1\rho}^{\infty}$, is the relaxation time at infinite spin-lock power, p_a and p_b are the fractional populations of conformations a and b (assuming two-site exchange), $\Delta\omega$ is the chemical shift difference between states a and b, $\omega_1 = \gamma B_1$ is the spin-lock power expressed in radians per second, and τ_{ex} is the lifetime for the exchange process (*23*, *24*). For more complicated multisite exchange, the detailed form of eq 1 will not hold, but the extracted parameter τ_{ex} does give a general indication of the time scale of the processes involved (*25*). For two-site exchange, τ_{ex} is related to the microscopic rate constants by

$$\frac{1}{\tau_{ex}} = k_{ex} = k_{a\rightarrow b} + k_{b\rightarrow a} \qquad (2)$$

where $k_{i\rightarrow j}$ is the rate constant for the conversion of state *i* to state *j*. This methodology has been applied to analysis of proton relaxation data in peptides (*24*, *25*) and DNA oligomers (*26*, *27*). More recently, $T_{1\rho}$ analyses of heteronuclear relaxation have been applied to specific sites in proteins (*28*−*31*).

The development of isotope-labeling techniques (*32*, *33*) allowed the use of ^{13}C and ^{15}N nuclei as probes of conformational dynamics in RNA (*34*−*37*). However, detailed analyses of microsecond-to-millisecond motions in nucleic acids using heteronuclear techniques are quite rare (*38*). The results in this paper therefore both provide insight into the dynamic properties of the leadzyme and demonstrate the usefulness of the power dependence of $T_{1\rho}$ relaxation techniques in studies of RNA.

MATERIALS AND METHODS

RNA Sample Preparation. A uniformly (>98%) ^{13}C, ^{15}N-labeled sample of the 30mer leadzyme RNA was prepared by in vitro transcription as previously described (*32*, *39*). The leadzyme sequence is shown in Figure 1A. The 1.2 mM sample was dissolved in 10 mM sodium phosphate buffer, > 99% D_2O, pH 5.5, 100 mM NaCl, 0.1 mM EDTA.

NMR Spectroscopy and Data Analysis. All spectra were acquired on Varian VXR or UnityInova 500 MHz spectrometers at a temperature of 25 °C. Aromatic ^{13}C $T_{1\rho}$ and T_1 relaxation were measured using nonconstant-time variations of published pulse sequences (*40*). These pulse sequences include elements to suppress cross-correlation effects and to minimize signal losses due to projection of magnetization onto tilted spin-lock axes. For $T_{1\rho}$ studies of adenine C2 carbons, the ^{13}C carrier was positioned at 151.2 ppm with a sweep width of 4500 Hz. A total of 56 complex t_1 increments of 32 transients each were collected with a recycle delay of 2 s, and a set of 14 different relaxation delays between 4 and 50 ms were used, with one time point acquired four times for error analysis. For the two highest spin lock powers, the longest relaxation delay was set to 28 ms to avoid sample heating. Six spin-lock powers ($\gamma B_1/2\pi$) between 0.9 and 6.5 kHz were used. For $T_{1\rho}$ studies of purine C8 carbons, the ^{13}C carrier was shifted to 139.5 ppm and 80 complex t_1 increments were collected. For measurement of ^{13}C T_1 values, spectra were acquired with a carrier of 145.6 ppm, a sweep width in t_1 of 3000 Hz, a relaxation delay of 1.9 s, using T_1 delays every 50 ms from 50−750 ms. In all cases, the proton carrier was set at the residual HDO signal, and low-power ^{13}C WALTZ decoupling was applied during acquisition (*41*). Spectra were processed with FELIX 97.0 (Molecular Simulations) using 3 Hz exponential line-broadening in t_2 and a cosine-squared window in t_1. Resolved cross-peaks were integrated in FELIX and employed previously determined resonance assignments for the leadzyme (*39*). Relaxation rates were extracted by fitting the data to single-exponential decays using Mathematica (Wolfram Research), including a constant offset in the case of T_1. Errors were propagated from the estimated uncertainty in peak intensity based on repetition of a single time point using Monte Carlo techniques (*42*).

Extraction of Dynamical Parameters. For off resonance cross-peaks, the spin-lock field must be considered as the effective field resulting from the applied B_1 field and the offset Ω:

$$\omega_{eff} = \sqrt{\omega_1^2 + \Omega^2} \qquad (3)$$

In addition, the observed $T_{1\rho}$ decay process will have contributions from both transverse and longitudinal relaxation, since the spin-lock axis is tilted out of the *xy* plane. This effect was taken into account using measured values of $R_1 = 1/T_1$ according to (*43*, *44*):

$$R_{1\rho}^{obs} = R_1 \cos^2 \theta + R_{1\rho} \sin^2 \theta \quad (4)$$

where $\theta = \tan^{-1}(\omega_1/\Omega)$ is the angle of the spin-lock axis from vertical. The maximum experimental offset was 550 Hz (for A18 C2), resulting in ranges for the tilt angles θ of 59−90° and 81−90° at 0.9 and 3.7 kHz, respectively.

For those aromatic carbon resonances in the leadzyme that showed variation of $R_{1\rho}$ with ω_{eff}, offset-corrected values were fit to eq 1 using the nonlinear Marquardt−Levenberg algorithm as implemented in Mathematica 3.0 (Wolfram Research) with Monte Carlo error propagation (*42*). Two-site exchange was assumed throughout. For the full three-parameter fit, the independent variables were τ_{ex}, $p_a p_b(\Delta\omega)^2$ and $T_{1\rho}^{\infty}$. The data generally covered an insufficient range of ω_1 to unambiguously define all three parameters. Thus the $T_{1\rho}^{\infty}$ values were calculated from the average $T_1/T_{1\rho}$ ratio for C8 resonances in the helical stem regions that showed no power dependence for $T_{1\rho}$. This ratio was used to calculate $T_{1\rho}^{\infty}$ values for other resonances from the measured T_1 value for the resonance (*24*). $T_{1\rho}$ values from the 3.7 kHz measurement were used because it is the highest power for curves extending past 40 ms. This independent estimate of one parameter allowed the use of a two-parameter fit to τ_{ex} and $p_a p_b(\Delta\omega)^2$. We note that assuming a constant $T_1/T_{1\rho}$ ratio amounts to neglecting variations in the carbon−hydrogen bond length and ^{13}C chemical shift anisotropy (CSA),[1] but does not require known values for these parameters. Ab initio calculations (*45*) and cross-correlation measurements (*46*) have hinted at variations in CSA between C2 and C8 groups, possibly leading to errors in $T_{1\rho}^{\infty}$ values for C2 resonances calculated using this procedure. The only C2 resonance in a helical region for which we have data, A12, however, showed a rate ratio within the range observed for helical C8 resonances, supporting the validity of this assumption. An estimate of the isotropic rotational correlation time was obtained from the $T_1/T_{1\rho}^{\infty}$ ratio for resonances in the helical stem that showed no evidence of exchange contributions when analyzed including dipole−dipole and chemical-shift anisotropy relaxation mechanisms (*19*, *47*). Using the fully anisotropic chemical shift tensor of $\sigma_z = 217.8$ ppm, $\sigma_y = 146.3$ ppm, $\sigma_x = 58.4$ ppm measured for guanine C8 (*48*) and a bond length of $r_{HC} = 1.09$ Å (*49*) yields an isotropic correlation time τ_m of 6.4 ± 0.2 ns at 25 °C for the leadzyme. From the limited relaxation data available, it is not possible to reliably determine the rotational diffusion anisotropy in this system.

RESULTS AND DISCUSSION

NMR Data and Relaxation Rates. Transverse and longitudinal relaxation rates could be obtained for the C8 resonances of 14 of the 19 purines in the leadzyme, the C6 resonances of 5 of the 11 pyrimidines, and the C2 resonances of 4 of the 7 adenines, for a total of 23 probes of base dynamics. All data were adequately fit to single-exponential decays. Representative relaxation curves for the G13 C8 resonance, which showed no variation of $R_{1\rho}$ with spin lock power, are shown in Figure 2A, and can be compared with the A25 C2 resonance, which shows a strong power dependence (Figure 2B) indicating a significant R_{ex} contribution. The reported transverse relaxation rates were corrected for the effects of offset using eq 4 (see Materials and Methods). Histograms of $R_{1\rho}$ relaxation rates at two selected spin-lock powers, as well as R_1 values, are shown in Figure 3. The complete set of determined relaxation rates is given in Table 1. Except for the resonances discussed below, only minor variations in $R_{1\rho}$ between 1.5 and 6.5 kHz were observed. For the 1.0 kHz (0.9 kHz for C2) data, by contrast, an enhancement in the relaxation rate of ∼10−15% was observed in most cases (Figure 3C). Although we cannot rule out the possibility that this observation reports on global conformational transition(s) with an exchange lifetime of tens to hundreds of milliseconds, it could also arise from systematic artifacts in the $T_{1\rho}$ measurement at very low spin-lock powers (see below). Thus caution should be used interpreting data where there are only small changes in relaxation rates with spin-lock power. Consistent with previous work at a single power (*39*), no significant differences were observed for relaxation rates of the pyrimidine C6 resonances. This is not surprising because all the resolved pyrimidine resonances are within helical secondary structure. The only pyrimidine resonance in the active-site internal loop, on residue C6, could not be analyzed due to spectral overlap. The C8 and C2 resonances from residues in the helical regions showed no evidence of exchange contributions from these relaxation data. By contrast, three purine C8 resonances (G7, A18, and G24) and one adenine C2 resonance (A25) in the internal loop or the GA_3 tetraloop, show a significant power dependence of $T_{1\rho}$ (Table 1 and

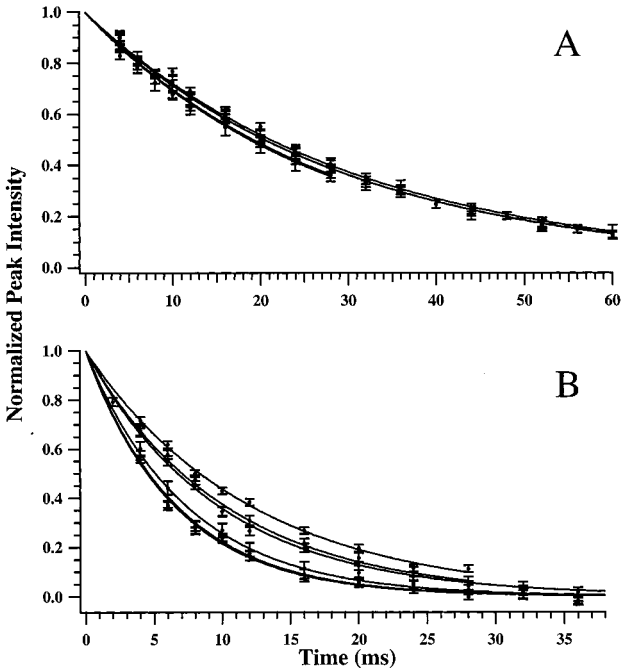

FIGURE 2: Representative ^{13}C $T_{1\rho}$ relaxation data on the leadzyme. Peak intensities versus relaxation delay are plotted at six different spin-lock powers for (A) G13 C8 and (B) A25 C2. Curves represent nonlinear least-squares fits to a single exponential.

[1] Abbreviations: CSA, chemical shift anisotropy; DMS, dimethyl sulfate; NOE, nuclear Overhauser effect.

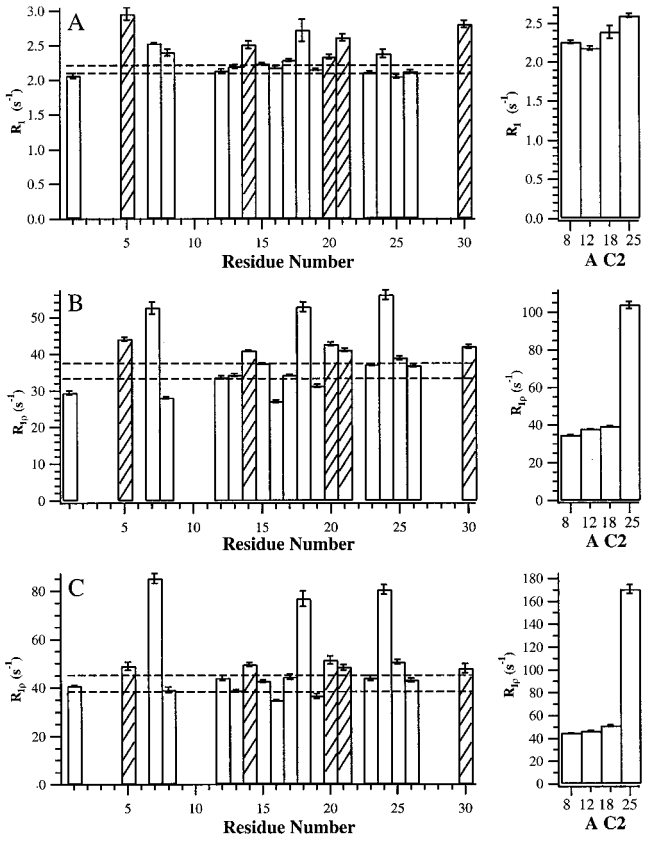

FIGURE 3: Histograms of the measured relaxation rates in the leadzyme are shown for (A) longitudinal relaxation, (B) transverse relaxation at 3.7 kHz spin-lock power, (C) transverse relaxation at 1.0 kHz spin-lock power. Error bars are based on Monte Carlo analysis of the data (see text). Purine C8 and C2 data are open bars and pyrimidine C6 data are hatched bars. Dotted horizontal lines represent the upper and lower data limits for C8 atoms in helical stems, which correspond to the expected range of relaxation rates for C8 resonances unaffected by internal motions.

Figures 2 and 3). This unambiguously demonstrates that these resonances are involved in an exchange process that contributes to their transverse relaxation. The observed dynamics in various regions of the molecule are described in more detail below.

Microsecond to Millisecond Motions in the Leadzyme. The power dependence of $R_{1\rho}$ for various resonances in the leadzyme are shown in Figure 4. For resonances that show changes in $R_{1\rho}$ with spin-lock power, the motional parameters can be extracted by nonlinear least-squares fitting to eq 1. This process is simplified by using the T_1 data to derive an independent estimate of $T_{1\rho}^{\infty}$, as described above. The calculated values of τ_{ex} and $p_a p_b(\Delta\omega)^2$ are given in Table 2 along with values of $\Delta\omega$ (ppm) corresponding to the case of $p_a = p_b = 0.5$, which is the minimum possible chemical shift change between states to account for the observed dynamics. The base of A25 in the leadzyme forms a AH^+-C base pair which leads to the adenine N1 having an unusual pK_a of 6.5 (*14*, *15*), thus Table 2 also lists $\Delta\omega$ for $p_a = 0.91$, $p_b = 0.09$, which corresponds to the populations for the protonation equilibrium for A25 N1 at pH=5.5.

Cross-Validation of Lifetimes Obtained from Line-Shape Analysis and Power Dependence of $T_{1\rho}$. For resonances that are in intermediate exchange on the chemical shift time scale, exchange lifetimes can be derived from line-shape analysis if the chemical shifts, populations and line widths of the exchanging states are known (*50*). However, it is rare to have data for all these parameters. The A25 C2 resonance in the leadzyme shows pH dependent line broadening which was previously assigned to the protonation/deprotonation equilibrium at the adjacent N1 site (*14*). Full line-shape analysis of the A25 ^{13}C resonance yielded an exchange lifetime between the protonated/deprotonated states of 31 ± 8 μs (*15*). Significantly, analysis of the power dependence of $T_{1\rho}$ for this resonance yields the same τ_{ex}, within experimental error (see Table 2). Using the previously determined values of p_a, p_b, and $\Delta\omega$ for this protonation/deprotonation equilibrium (*15*, *51*) it is possible to independently determine the $p_a p_b$-$(\Delta\omega)^2$ parameter (3.1×10^6), which is in excellent agreement with the value determined here from the analysis of the $T_{1\rho}$ data (Table 2). The agreement for these dynamical parameters obtained by the two different methods helps validate the power dependence of $T_{1\rho}$ technique and increases our confidence in the analysis of the $T_{1\rho}$ data at other sites in the leadzyme.

Exchanging Hydrogen Bonds in the GA$_3$ Tetraloop. In the GAAA tetraloop of the leadzyme, G15 stacks on the 5′ strand and is followed by a sharp turn in the backbone at G15pA16, leaving the three adenine bases to stack on the 3′ strand (*7*, *52*, *53*). This structure is reflected in the dynamical data reported here (Figure 3B), for which the capping residue A16 has a longer $T_{1\rho}$ than the helical regions, indicating rapid (ps−ns) disorder. This base was previously proposed to be disordered from structural and phylogenetic data (*52*). The base of A17 is involved in stacking interactions on both sides and is protected from chemical modification upon RNA folding (*7*, *39*) and shows no evidence for dynamics at the C8 site. Previous studies on the leadzyme showed a larger $R_{1\rho}$ for the C8 resonance of A18 compared to resonances in helical regions (*39*), suggesting an exchange contribution. This is confirmed by the $R_{1\rho}$ curve in Figure 4B, which has a clear power dependence of the relaxation rate, and yields an exchange lifetime of 80 μs (Table 2). This shows that the stable GAAA tetraloop is undergoing exchange between at least two conformers of roughly comparable free energy. We have previously proposed that the GNRA tetraloops are stabilized by a heterogeneous, dynamic network of hydrogen bonds (*53*). This hypothesis helps explain the relatively small impact of deletion of individual hydrogen-bonding groups on the thermodynamic stability of the loop (*54*). The first and fourth nucleotides in the tetraloop, G15 and A18, are involved in a sheared anti-anti G−A base pair (*53*). Figure 5 illustrates that a reshuffling of hydrogen bonds from the depicted arrangement for the G15-A18 base pair would be expected to have a significant effect on the chemical shift of A18 C8 (adjacent to a hydrogen-bonded nitrogen), a smaller effect on A18 C2, and little direct effect on G15 C8, which is on the opposite face of the guanine base from the groups involved in hydrogen bonds. Intriguingly, this is the same relative pattern of effects observed for these resonances in the $R_{1\rho}$ data (see Table 1 and Figure 4B). In addition to the significant R_{ex} for A18 C8 discussed above, a smaller but significant effect is observed for A18 C2 (Figure 4B and Table 2). The C8 resonance of G15, by contrast, shows no significant change in $R_{1\rho}$ over the range of field strengths used here. In summary, the spin-relaxation analysis presented here strongly indicates that the GAAA tetraloop takes on multiple conformations on the microsecond time scale, and is consistent with the previous model of a

Table 1: ^{13}C Relaxation Rates in the Leadzyme

		$R_{1\rho}$ (s^{-1}) at given B_1 field					
C6/C8	R_1 (s^{-1})	1.0 kHz	1.6 kHz	2.6 kHz	3.7 kHz	5.2 kHz	6.5 kHz
G1	2.06 ± 0.04	40.8 ± 0.3	28 ± 1	31.8 ± 0.5	29.5 ± 0.6	30.1 ± 0.4	26.9 ± 0.7
C5	2.96 ± 0.09	49 ± 2	44.2 ± 0.6	47 ± 1	44.1 ± 0.5	48 ± 1	50 ± 1
G7	2.54 ± 0.01	85 ± 2	75 ± 4	61 ± 2	53 ± 3	54 ± 2	50.1 ± 0.4
A8	2.40 ± 0.05	39 ± 1	31.7 ± 0.6	29.5 ± 0.5	28.2 ± 0.3	30 ± 2	29.9 ± 0.9
A12	2.14 ± 0.03	44 ± 1	32.4 ± 0.4	34.9 ± 0.3	33.7 ± 0.4	35 ± 1	35.5 ± 0.3
G13	2.20 ± 0.03	38.8 ± 0.5	34.6 ± 0.5	34.7 ± 0.9	34.3 ± 0.4	37 ± 1	36.3 ± 0.4
C14	2.52 ± 0.05	49.7 ± 0.9	44 ± 1	44.2 ± 0.4	41.1 ± 0.1	43.4 ± 0.6	44.2 ± 0.9
G15	2.24 ± 0.02	42.8 ± 0.6	39.6 ± 0.3	38.6 ± 0.9	37.5 ± 0.2	43.3 ± 0.9	41.4 ± 0.8
A16	2.19 ± 0.02	34.9 ± 0.3	28.2 ± 0.4	28.1 ± 0.3	27.2 ± 0.3	28.3 ± 0.7	28.1 ± 0.4
A17	2.30 ± 0.02	45 ± 1	35.0 ± 0.5	34.5 ± 0.5	34.3 ± 0.1	35.0 ± 0.9	34.3 ± 0.1
A18	2.7 ± 0.2	77 ± 3	73 ± 5	60 ± 2	53 ± 1	51 ± 1	50 ± 1
G19	2.16 ± 0.02	37 ± 1	31.4 ± 0.3	31.5 ± 0.7	31.4 ± 0.4	33.3 ± 0.6	33.5 ± 0.3
U20	2.34 ± 0.03	52 ± 2	44.4 ± 0.3	43.3 ± 0.7	42.8 ± 0.5	49 ± 1	47 ± 1
U21	2.62 ± 0.05	49 ± 1	48.3 ± 0.5	42 ± 1	41.2 ± 0.5	44 ± 2	43 ± 1
G23	2.12 ± 0.02	44 ± 1	39.8 ± 0.4	38.7 ± 0.9	37.2 ± 0.3	38 ± 1	38.5 ± 0.5
G24	2.39 ± 0.06	81 ± 2	75 ± 4	78 ± 1	56 ± 1	68 ± 3	63 ± 4
A25	2.05 ± 0.03	50.7 ± 0.9	43.6 ± 0.6	42.2 ± 0.6	39.0 ± 0.5	43 ± 1	38.3 ± 0.6
G26	2.13 ± 0.03	43.1 ± 0.8	39.4 ± 0.7	39 ± 1	36.9 ± 0.4	38 ± 1	38.1 ± 0.3
C30	2.82 ± 0.05	48 ± 2	46.2 ± 0.9	44 ± 1	42.1 ± 0.5	49.2 ± 0.9	48 ± 1
Ade C2	R_1 (s^{-1})	0.9 kHz	1.7 kHz	2.6 kHz	3.7 kHz	5.2 kHz	6.5 kHz
A8	2.26 ± 0.02	44.8 ± 0.4	38.3 ± 0.5	35.7 ± 0.7	34.8 ± 0.2	36.8 ± 0.3	35.6 ± 0.2
A12	2.18 ± 0.03	46.5 ± 0.7	40.6 ± 0.9	40 ± 1	38.0 ± 0.2	39.5 ± 0.4	39.0 ± 0.8
A18	2.39 ± 0.08	51.3 ± 0.6	46.1 ± 0.9	42.6 ± 0.2	39.4 ± 0.2	40.6 ± 0.5	38.8 ± 0.3
A25	2.60 ± 0.02	171 ± 4	160 ± 2	138 ± 5	104 ± 2	98 ± 2	83 ± 1

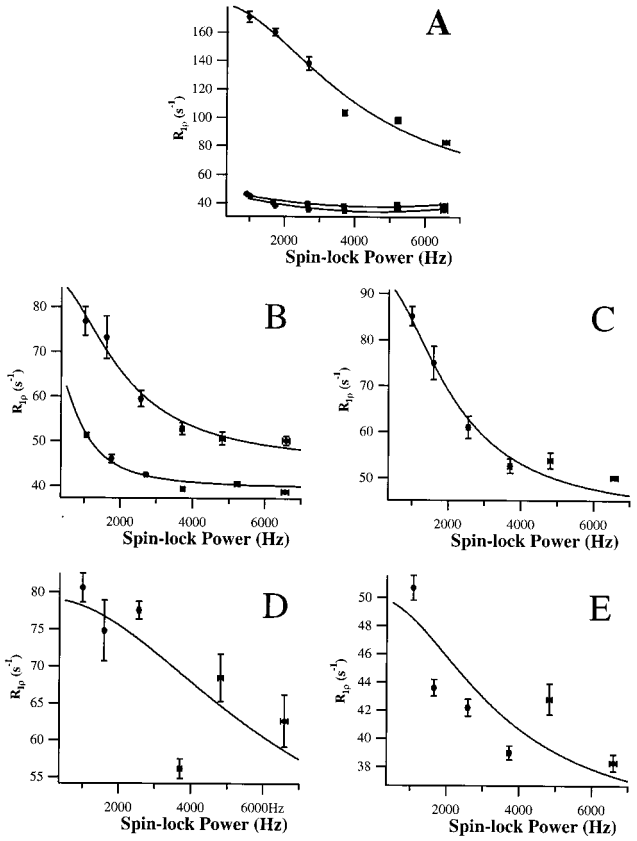

FIGURE 4: Power dependence of ^{13}C transverse relaxation rates ($R_{1\rho} = 1/T_{1\rho}$) as a function of applied spin-lock strength, ω_1^{eff}, in hertz. (A) A25 C2, upper curve; A12 C2 and A8 C2, lower curves. (B) A18 C8, upper curve; A18 C2, lower curve. (C) G7 C8. (D) G24 C8. (E) A25 C8. Curves shown are fits to eq 1 except for the lower two curves in panel A, which are third-degree polynomials meant only to guide the eye.

dynamically interconverting network of hydrogen bonds that stabilize this tetraloop (*53*).

Multiple Independent Motions Near the Active Site. In addition to the effects observed for A25 C2 discussed above, previous measurements indicated enhanced $T_{1\rho}$ relaxation for the G24 and G7 C8 resonances in the leadzyme active-site (Figure 4, panels C and D; ref *39*). The results for the power dependence of $T_{1\rho}$ obtained here (Table 2) confirm exchange contributions affecting these groups, but do not support a hypothesis that all these active site ^{13}C resonances are reporting on the same conformational equilibrium. Specifically, the exchange lifetime for G7 C8 is incompatible with that for the dynamics affecting A25 C2. In addition, the extracted value of $p_a p_b(\Delta\omega)^2$ for G7 C8 requires a minimal chemical shift change of 2.1 ppm, or 3.6 ppm for $p_a/p_b = 10$, which are both substantially larger than the value from the pH titration (Table 2). Thus, the chemical shift of G7 C8 is affected by another exchange process in addition to the opening of the AH^+-C base pair, although the protonation equilibrium may well contribute a portion of the R_{ex} term for this resonance. A complicated pattern of conformational dynamics for this residue is consistent with the observation of NOE cross-peaks to G7 C8 that are incompatible with a single structure (*7*). The adjacent residue, A8 C8, by contrast, shows picosecond to nanosecond dynamics as reflected in a decreased value for $R_{1\rho}$ (Table 1).

The G24 C8 resonance, which is unaffected by pH in the range of 4.4−8.3 (*51*), also shows a power dependence of $T_{1\rho}$ (Figure 4D and Table 2). Interestingly, the N7 site on this residue is protected from chemical modification with dimethyl sulfate (DMS) upon ribozyme folding (*39*). Therefore, the observed exchange process either involves transitions between two (or more) significantly populated conformations, both of which sequester N7, or the NMR data are dominated by exchange with a very low population conformation that is not efficiently sampled in the chemical probing data (for example, if $p_b = 0.05$, the $\Delta\omega$ calculated from the $T_{1\rho}$ data is >7 ppm). It appears that the dynamics observed for G24 C8 are distinct from both the pH-dependent AH^+-C

Table 2: Chemical Exchange Parameters Determined from Analysis of the Power Dependence of $T_{1\rho}$ in the Leadzyme[a]

	$R_{1\rho}$ (s^{-1})	τ_{ex} (μs)	$p_a p_b(\Delta\omega)^2$ ($\times 10^5$)	$\Delta\omega_{min}$[b]	$\Delta\omega_{10:1}$[c]	pK_a[d]	$\Delta\omega_{pH}$[d]
G7 C8	42 ± 2.6	76 ± 13	6.8 ± 1.0	2.1 ± 0.2	3.6 ± 0.3	6.2 ± 0.1	1.0 ± 0.1
A18 C8	45 ± 3.9	80 ± 20[e]	5.2 ± 1.7	1.8 ± 0.3	N/A	N/A	N/A
A18 C2	40 ± 2.8	190 ± 80[e]	1.6 ± 0.4	1.1 ± 0.1	N/A	N/A	N/A
G24 C8	40 ± 2.7	25 ± 4	16 ± 3.0	3.2 ± 0.3	5.6 ± 0.5	N/A	<0.2
A25 C2	43 ± 2.7	40 ± 1.8	34 ± 2.0	4.6 ± 0.1	8.1 ± 0.2	6.5 ± 0.1[f]	7.8 ± 0.1[f]
A25 C8	34 ± 2.2	47 ± 18	3.4 ± 1.1	1.4 ± 0.2	2.5 ± 0.4	6.4 ± 0.1	2.1 ± 0.1

[a] Data were extracted from two parameter fits to eq 1. All chemical shift values ($\Delta\omega$) in parts per million. [b] Calculated from $p_a p_b(\Delta\omega)^2$ using $p_a = p_b = 0.5$. [c] Calculated from $p_a p_b(\Delta\omega)^2$ using $p_a = 0.91$, $p_b = 0.09$. [d] Derived from chemical shift vs pH data in ref *51*. [e] Errors are reported from the covariation matrix due to poor numerical conditioning in the Monte Carlo procedure. [f] Ref *15*.

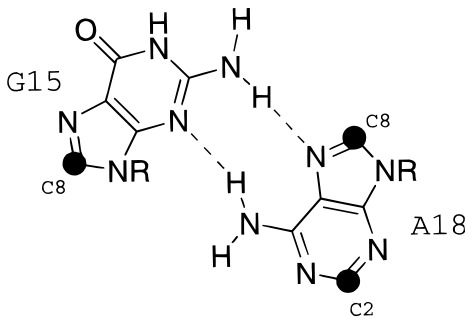

FIGURE 5: Schematic structure of the G15-A18 sheared base pair found in the GAAA tetraloop in the leadzyme (adapted from ref *53*).

base pair opening and the exchange process reported on by G7 C8. The conformational energy landscape for the internal loop of the leadzyme is thus quite complex, with different NMR probes reporting on a variety of processes interconverting among several populated states.

Finally, we examined the power dependence of $T_{1\rho}$ data for A25 C8 to determine if this resonance is affected by the AH^+−C base pair opening dynamics or by any other exchange process (Figure 4E). Indeed, this resonance exhibits a moderate R_{ex} term yielding an exchange lifetime of 47 ± 18 μs (Table 2), consistent with the AH^+−C base pair opening as reported by A25 C2. In addition, previous data reported a chemical shift change of +1.9 ppm for this resonance upon protonation (*15*, *51*), in reasonable agreement with the $|\Delta\omega|$ of 2.5 ± 0.4 ppm obtained from the $T_{1\rho}$ data using $p_a/p_b = 10$ (Table 2). Thus the entire R_{ex} contribution for A25 C8 is explained by the exchange between the protonated and deprotonated states of the A25 base. We also note that in monomeric 5′-AMP the C8 chemical shift changes by approximately +2.5 ppm upon protonation at N1 (*15*), implying that the source of the chemical shift change at A25 C8 in the leadzyme is polarization effects propagating from N1, rather than a conformational change in the immediate vicinity of the C8 atom that affects the chemical shift.

Despite the complexity of the internal loop dynamics described here, is it possible to make some conclusions about the nature of the internal motions for this region. In earlier work, we noted that G24 C8 showed essentially no pH dependence of chemical shift, indicating that the environment of this atom is not affected by the opening of the AH^+25-C6 base pair (*39*). Here we showed that the $T_{1\rho}$ data for the A25 C8 is completely accounted for by electronic changes within the adenine base upon deprotonation, and we also observed no power dependence of $T_{1\rho}$ for G26 C8 (Table 1). The simplest explanation of these results is that the structure of the 3′ (ribozyme) strand of the internal loop, residues 23−26, is not significantly affected by the transition between the open and closed states of the AH^+25-C6 base pair. Therefore the base-pair opening dynamics for these residues, observed previously by line-shape analysis (*15*) and here by the power dependence of $T_{1\rho}$, consists of conformational changes of the 5′ (substrate) strand residues. Specifically movement of the base of C6 would expose the protonated A25 N1 to solvent, leading to hydrogen exchange.

A Mechanistic Hypothesis: Base Pair Breakage along the Reaction Coordinate. One of the challenges in interpreting conformational fluctuations identified by NMR techniques is to try to understand which of these fluctuations are critical for function, in this case catalytic activity of the leadzyme. Sufficient phylogenetic and modification data are available for the leadzyme to allow initial models to be proposed. We focus here on conformational dynamics associated with the protonation/deprotonation equilibrium of A25 (*15*), which we propose consists of motion of the base of C6 relative to the more static A25 on the 3′ strand. The scissile phosphate group in the leadzyme is immediately adjacent to C6 (Figure 1), therefore conformational changes involving this base might affect the structure of the reactive groups. It is interesting to note that substitution of the AH^+−C base pair with either an isosteric G−U pair or a G−C pair results in inactive ribozyme (*39*, *55*), whereas replacement of the protonated A with an abasic site is fully compatible with catalysis (*56*). One explanation for these results is that there is no base pair formed in conformations leading to the transition state. This hypothesis explains the inactivity of the G−C and G−U base pairs at this site, since the increased stability of these base pairs compared with AH^+−C would increase the kinetic barrier to an active conformation. In the abasic-25 variant, no such barrier would be present. Further biochemical studies are required to confirm this hypothesis.

Two conformations were observed for the active site in the X-ray crystal structure of the leadzyme (*8*), and the conformation closest to having an in-line attack configuration contains a Ba^{2+} ion on the N1 of A25. Thus the protonated AH^+−C base pair, unambiguously identified in the NMR studies, is not observed in the X-ray structure even though it would be the predominant protonation state in solution at the pH used in the crystallization (*8*). However since the adenine at position 25 is dispensable for catalysis, and may be replaced by an abasic site without loss of activity (*56*), the mechanistic relevance of either the specific ion ligation observed crystallographically, or the protonated AH^+−C base pair observed by NMR, is uncertain. In a molecular modeling study of the active conformation of the leadzyme, the AH^+−C base pair observed in the ground state in solution

is replaced by a base triple formed by C6, G9, and G24 (*57*). In the X-ray structure of a putative conformational intermediate in the hammerhead ribozyme, the base (C17) immediately 5′ to the cleavage site is not in its ground state conformation, which involves a noncanonical base pair with C3 on the opposing strand, but instead moves completely out of the helical structure thus causing a conformational rearrangement of the active-site functional groups (*58*). The placement of a less stable noncanonical base pair 5′ to the scissile phosphate, leading to a reduction in the energetic barrier for conformational rearrangement, may be a generally useful catalytic strategy for small ribozymes.

Extracting Dynamical Information from the Power Dependence of $T_{1\rho}$. The studies reported here on the dynamics of the leadzyme employed spin-lock powers of 1.0−6.5 kHz, which allows analysis of exchange lifetimes ranging from approximately 10^{-5} to 10^{-3} s. This range is limited on the short time scale side by power deposition in the NMR probe. The application of off-resonance spin-locking fields to increase the magnitude of ω_1^{eff} (*59*−*61*) should also aid in studying shorter time scale motions. On the low-power side, we observed oscillatory behavior in $T_{1\rho}$ decay curves obtained substantially below 1.0 kHz (data not shown), which we tentatively attribute to contributions arising from residual scalar coupling interactions with neighboring nuclei. The use of CPMG-type sequences may extend the range of the analysis to several millisecond lifetimes (*62*, *63*). The application of ^{1}H WALTZ decoupling during the relaxation delay may also alleviate problems arising from ^{13}C-^{1}H scalar coupling interactions (*29*).

In this study on the leadzyme, we focused on ^{13}C nuclei that are not involved in covalent ^{13}C−^{13}C bonds (with the exception of pyrimidine C6 atoms, which are well separated in chemical shift from the adjacent C5s, and were only interpreted in a qualitative sense). For many carbon atoms in RNA, however, scalar and dipolar ^{13}C-^{13}C couplings are likely to interfere with the acquisition and/or interpretation of relaxation data in uniformly labeled samples. Interference due to Hartmann−Hahn transfer (*40*) will be a problem for the ribose carbons, which have similar chemical shifts and substantial scalar coupling constants. It is likely that specific (*32*, *64*−*66*), fractional (*46*), and/or alternating site (*67*, *68*) isotopic labeling will be required for complete analysis of ribose carbon dynamics in RNA.

CONCLUSIONS

Conformational dynamics appear to play a key role in the catalytic function of the leadzyme. In this report we demonstrate how measurements of the power dependence of ^{13}C $T_{1\rho}$ data can be used to probe the extent, time scale, and molecular nature of conformational dynamics in RNA. The conformational dynamics for protonation of the A25 base in the active site of the leadzyme were probed by the ^{13}C $T_{1\rho}$ experiments and the results were in excellent agreement with the exchange lifetime previously determined by lineshape analysis (*15*). These data therefore provide an extremely valuable calibration for conformational dynamics determined by analysis of the power dependence of ^{13}C $T_{1\rho}$ technique. The ^{13}C $T_{1\rho}$ relaxation data obtained here revealed a variety of conformation dynamics for the active site internal loop and the GAAA tetraloop in the leadzyme. These studies reemphasize that a complete understanding of the mechanism of catalysis in RNAs requires detailed studies of both the structure and dynamics of the molecule. The results presented here provide an important step toward achieving this goal for the leadzyme, and also demonstrate how the power dependence of $T_{1\rho}$ data can be used to probe microsecond-to-millisecond time scale conformation dynamics in RNAs.

ACKNOWLEDGMENT

The authors thank Dr. Pascale Legault for preparing the isotopically labeled leadzyme sample, P. Jason Booker for assistance with data collection, and Drs. Paul Hanson and Fiona Jucker for helpful discussions.

REFERENCES

1. Ferré-D'Amaré, A. R., and Doudna, J. A. (1999) *Annu. Rev. Biophys. Biomol. Struct. 28*, 57−73.
2. Hermann, T., and Patel, D. J. (1999) *J. Mol. Biol. 294*, 829−849.
3. Moore, P. B. (1999) *Annu. Rev. Biochem. 68*, 287−300.
4. Pley, H. W., Flaherty, K. M., and McKay, D. B. (1994) *Nature 372*, 68−74.
5. Scott, W. G., Finch, J. T., and Klug, A. (1995) *Cell 81*, 991−1002.
6. Scott, W. G., Murray, J. B., Arnold, J. R. P., Stoddard, B. L., and Klug, A. (1996) *Science 274*, 2065−2069.
7. Hoogstraten, C. G., Legault, P., and Pardi, A. (1998) *J. Mol. Biol. 284*, 337−350.
8. Wedekind, J. E., and McKay, D. B. (1999) *Nat. Struct. Biol. 6*, 261−268.
9. Steitz, T. A., and Steitz, J. A. (1993) *Proc. Natl. Acad. Sci. U.S.A. 90*, 6498−6502.
10. Frankel, A. D. (1999) *Nat. Struct. Biol. 6*, 1081−1083.
11. Green, R., and Noller, H. (1997) *Annu. Rev. Biochem. 66*, 679−716.
12. Madhani, H. D., and Guthrie, C. (1994) *Annu. Rev. Genet. 28*, 1−26.
13. Nilsen, T. W. (1998) in *RNA Structure and Function* (Simons, R. W., and Grunberg-Manago, M., Eds.) pp 279−307, Cold Spring Harbor Laboratory Press, Plainview, NY.
14. Legault, P., and Pardi, A. (1994) *J. Am. Chem. Soc. 116*, 8390−8391.
15. Legault, P., and Pardi, A. (1997) *J. Am. Chem. Soc. 119*, 6621−6628.
16. Wagner, G., and Wüthrich, K. (1986) *Methods Enzymol. 131*, 307−326.
17. Dayie, K. T., Wagner, G., and Lefèvre, J. F. (1996) *Annu. Rev. Phys. Chem. 47*, 243−282.
18. Palmer, A. G., III (1997) *Curr. Opin. Struct. Biol. 7*, 732−737.
19. Kay, L. E. (1998) *Nat. Struct. Biol. 5*, 513−517.
20. Lipari, G., and Szabo, A. (1982) *J. Am. Chem. Soc. 104*, 4546−4559.
21. Kay, L. E., Torchia, D. A., and Bax, A. (1989) *Biochemistry 28*, 8972−8979.
22. Tjandra, N., Wingfield, P., Stahl, S., and Bax, A. (1996) *J. Biomol. NMR 8*, 273−284.
23. Deverell, C., Morgan, R. E., and Strange, J. H. (1970) *Mol. Phys. 18*, 553−559.
24. Blackledge, M. J., Brüschweiler, R., Griesinger, C., Schmidt, J. M., Xu, P., and Ernst, R. R. (1993) *Biochemistry 32*, 10960−10974.
25. Kopple, K. D., Wang, Y.-S., Cheng, A. G., and Bhandary, K. K. (1988) *J. Am. Chem. Soc. 110*, 4168−4176.
26. Wang, Y.-S., and Ikuta, S. (1989) *J. Am. Chem. Soc. 111*, 1243−1248.
27. Lane, A. N., Bauer, C. J., and Frenkiel, T. A. (1993) *Eur. Biophys. J. 21*, 425−431.
28. Szyperski, T., Luginbühl, P., Otting, G., Güntert, P., and Wüthrich, K. (1993) *J. Biomol. NMR 3*, 151−164.
29. Habazettl, J., Myers, L. C., Yuan, F., Verdine, G. F., and Wagner, G. (1996) *Biochemistry 35*, 9335−9348.

30. Akke, M., Liu, J., Cavanagh, J., Erickson, H. P., and Palmer, A. G., III (1998) *Nat. Struct. Biol. 5*, 55−59.
31. Banci, L., Felli, I. C., and Kouloughotis, D. (1998) *J. Biomol. NMR 12*, 307−318.
32. Nikonowicz, E. P., Sirr, A., Legault, P., Jucker, F. M., Baer, L. M., and Pardi, A. (1992) *Nucleic Acids Res. 20*, 4507−4513.
33. Batey, R. T., Inada, M., Kujawinski, E., Puglisi, J. D., and Williamson, J. R. (1992) *Nucleic Acids Res. 20*, 4515−4523.
34. King, G. C., Harper, J. W., and Xi, Z. (1995) *Methods Enzymol. 261*, 436−450.
35. Akke, M., Fiala, R., Jiang, F., Patel, D., and Palmer, A. G., III (1997) *RNA 3*, 702−709.
36. Hall, K. B., and Tang, C. (1998) *Biochemistry 37*, 9323−9332.
37. Zimmermann, G. R., Jenison, R. D., Wick, C. L., Simorre, J.-P., and Pardi, A. (1997) *Nat. Struct. Biol. 4*, 644−649.
38. Gaudin, F., Chanteloup, L., Thuong, N. T., and Lancelot, G. (1997) *Magn. Reson. Chem. 35*, 561−565.
39. Legault, P., Hoogstraten, C. G., Metlitzky, E., and Pardi, A. (1998) *J. Mol. Biol. 284*, 325−335.
40. Yamazaki, T., Muhandiram, D. R., and Kay, L. E. (1994) *J. Am. Chem. Soc. 116*, 8266−8278.
41. Shaka, A. J., Keeler, J., Frienkiel, T., and Freeman, R. (1983) *J. Magn. Reson. 52*, 335−338.
42. Press, W. H., Flannery, B. P., Teukolsky, S. A., and Vetterling, W. T. (1988) *Numerical Recipes in C*, Cambridge University Press, Cambridge.
43. James, T. L., Matson, G. B., and Kuntz, I. D. (1978) *J. Am. Chem. Soc. 100*, 3590−3594.
44. Davis, D. G., Perlman, M. E., and London, R. E. (1994) *J. Magn. Reson. B 104*, 266−275.
45. Sitkoff, D., and Case, D. A. (1998) *Prog. NMR Spectrosc. 32*, 165−190.
46. Boisbouvier, J., Brutscher, B., Simorre, J.-P., and Marion, D. (1999) *J. Biomol. NMR 14*, 241−252.
47. Abragam, A. (1961) *The Principles of Nuclear Magnetism*, Oxford University Press, Oxford.
48. Tang, P., Santos, R. A., and Harbison, G. S. (1989) *Adv. Magn. Reson. 13*, 225−255.
49. Saenger, W. (1984) *Principles of Nucleic Acid Structure*, Springer-Verlag, New York.
50. Lian, L.-Y., and Roberts, G. C. K. (1993) in *NMR of Macromolecules: A Practical Approach* (Roberts, G. C. K., Ed.) pp 153−182, Oxford University Press, Oxford.
51. Legault, P. (1995) Ph.D. Thesis, University of Colorado, Boulder, CO.
52. Heus, H. A., and Pardi, A. (1991) *Science 253*, 191−194.
53. Jucker, F. M., Heus, H. A., Yip, P. F., Moors, E. H. M., and Pardi, A. (1996) *J. Mol. Biol. 264*, 968−980.
54. SantaLucia, J., Kierzek, R., and Turner, D. H. (1992) *Science 256*, 217−219.
55. Pan, T., Dichtl, B., and Uhlenbeck, O. C. (1994) *Biochemistry 33*, 9561−9565.
56. Chartrand, P., Usman, N., and Cedergren, R. (1997) *Biochemistry 36*, 3145−3150.
57. Lemieux, S., Chartrand, P., Cedergren, R., and Major, F. (1998) *RNA 4*, 739−749.
58. Murray, J. B., Terwey, D. P., Maloney, L., Karpeisky, A., Usman, N., Beigelman, L., and Scott, W. G. (1998) *Cell 92*, 665−673.
59. Akke, M., and Palmer, A. G., III (1996) *J. Am. Chem. Soc. 118*, 911−912.
60. Zinn-Justin, S., Berthault, P., Guenneugues, M., and Desvaux, H. (1997) *J. Biomol. NMR 10*, 363−372.
61. Mulder, F. A. A., de Graaf, R. A., Kaptein, R., and Boelens, R. (1998) *J. Magn. Reson. 131*, 351−357.
62. Orekhov, V. Y., Pervushin, K. V., and Arseniev, A. S. (1994) *Eur. J. Biochem. 219*, 887−896.
63. Loria, J. P., Rance, M., and Palmer, A. G., III (1999) *J. Am. Chem. Soc. 121*, 2331−2332.
64. Williamson, J. R., and Boxer, S. G. (1989) *Biochemistry 28*, 2819−2831.
65. Gaudin, F., Paquet, F., Chanteloup, L., Beau, J.-M., Thuong, N. T., and Lancelot, G. (1995) *J. Biomol. NMR 5*, 49−58.
66. Kojima, C., Ono, A., Kainosho, M., and James, T. L. (1998) *J. Magn. Reson. 135*, 310−333.
67. LeMaster, D. M., and Cronan, J. E., Jr. (1982) *J. Biol. Chem. 257*, 1224−1230.
68. LeMaster, D. M., and Kushlan, D. M. (1996) *J. Am. Chem. Soc. 118*, 9255−9264.

BI0007627